

Microsecond Exchange of Internal Water Molecules in Bacteriorhodopsin

Michael Gottschalk¹, Norbert A. Dencher² and Bertil Halle^{1*}

¹Physical Chemistry 2, Lund University, PO Box 124 SE-22100 Lund, Sweden

²Physical Biochemistry Darmstadt University of Technology, Petersenstr. 22 D-64287 Darmstadt Germany

The proton-conducting pathway of bacteriorhodopsin (BR) contains at least nine internal water molecules that are thought to be key players in the proton translocation mechanism. Here, we report the results of a multinuclear (¹H, ²H, ¹⁷O) magnetic relaxation dispersion (MRD) study with the primary goal of determining the rate of exchange of these internal water molecules with bulk water. This rate is of interest in current attempts to elucidate the molecular details of the proton translocation mechanism. The relevance of water exchange kinetics is underscored by recent crystallographic findings of substantial variations in the number and locations of internal water molecules during the photocycle. Moreover, internal water exchange is believed to be governed by conformational fluctuations in the protein and can therefore provide information about the thermal accessibility of functionally important conformational substates. The present ²H and ¹⁷O MRD data show that at least seven water molecules, or more if they are orientationally disordered, in BR have residence times (inverse exchange rate constant) in the range 0.1–10 μs at 277 K. At least five of these water molecules have residence times in the more restrictive range 0.1–0.5 μs. These results show that most or all of the deeply buried water molecules in BR exchange on a time-scale that is short compared to the rate-limiting step in the photocycle. The MRD measurements were performed on BR solubilized in micelles of octyl glucoside. From the MRD data, the rotational correlation time of detergent-solubilized BR was determined to 35 ns at 300 K, consistent with a monomeric protein in complex with about 150 detergent molecules. The solubilized protein was found to be stable in the dark for at least eight months at 277 K.

© 2001 Academic Press

Keywords: bacteriorhodopsin; octyl glucoside; water exchange; water residence time; magnetic relaxation dispersion

*Corresponding author

Introduction

Bacteriorhodopsin (BR), the light-driven proton pump of halophilic archaeobacteria, has become the paradigm of membrane proteins in general and ion pumps in particular.^{1–4} Proton translocation from the cytoplasm to the extracellular medium proceeds *via* a series of acidic and basic side-chains located in the central region surrounded by the seven membrane-spanning α -helices of BR. A reti-

nal molecule linked to Lys216 *via* a protonated Schiff base divides this conduction “channel” into two half-channels. In the following, we refer to these as the extracellular (EC) channel and the cytoplasmic (CP) channel.

Internal water molecules have long been recognized as key players in the proton conduction mechanism of BR.^{5–7} By neutron diffraction, 7 ± 1 water molecules were localized in the proton conduction pathway of BR in partly dehydrated purple membrane films (15% relative humidity, room temperature).^{8,9} Some of these internal water molecules are present even at 0% relative humidity, indicating that they interact strongly with the protein.⁸ More recently, high-resolution X-ray diffraction of fully hydrated BR, reconstituted in a cubic liquid crystal at 100 K, has revealed seven water molecules in the EC channel and two in the

Abbreviations used: BR, bacteriorhodopsin; cmc, critical micelle concentration; CP, cytoplasmic; EC, extracellular; FC, field cycling; OG, *n*-octyl- β -D-glucoside; MRD, magnetic relaxation dispersion; SDF, spectral density function.

E-mail address of the corresponding author: bertil.halle@fkem2.lth.se

CP channel.^{10–12} Most or all of these water molecules are likely to be involved directly in the proton translocation mechanism. High-resolution crystal structures are now also available for some of the spectroscopically identified intermediates in the photocycle.^{12–15}

While the locations and inferred H-bond connectivities of these internal water molecules are essential, one would also like to quantify their mobility. Such knowledge is particularly relevant, as it is now known that the number and locations of internal water molecules undergo substantial variations during the photocycle.^{12–15} For example, knowledge of the time-scale on which the water molecule H-bonded to the Schiff base exchanges with bulk water might provide insights about the mechanism of proton translocation. Furthermore, the exchange rates of trapped water molecules report on the kinetics of thermally activated conformational fluctuations in the protein.¹⁶ Although the kinetics of the exchange of the Schiff base proton with bulk water have been studied,^{17,18} no direct information about the exchange rates of internal water molecules in BR is available. Here, we describe a magnetic relaxation dispersion study that provides such information.

Intact BR in purple membrane fragments has been studied by a variety of techniques, including solid-state NMR of ¹³C-labeled residues^{19–21} and pulsed-gradient spin-echo NMR of translational diffusion of interlamellar water.²² For solution NMR studies, it is necessary to solubilize BR in detergent micelles.²³ While some solution NMR studies of isotope-labeled BR solubilized in detergent micelles have been performed,^{24–27} we are not aware of any previous NMR study of the internal hydration of BR or any other membrane protein.

In the past decade, two complementary NMR methods have been used extensively for studying protein hydration in solution. One of these measures spectral peak intensities related to the rate of intermolecular magnetic cross-relaxation between water and protein protons,²⁸ while the other directly measures the magnetic auto-relaxation rates of one or more nuclear isotopes in the water molecule over a wide field/frequency range.^{29,30} The cross-relaxation method relies on high-resolution spectra and has therefore not yet been applied to proteins as large as (solubilized) BR. The magnetic relaxation dispersion (MRD) method does not suffer from this limitation, but has not been applied to a membrane protein. A ²H MRD study of purple membrane sheets at low water content has been reported briefly,³¹ but, due to the nature of the sample and the contribution from labile deuterons, it could not provide unambiguous information about BR hydration.

In the present work, we use ¹⁷O, ²H, and ¹H MRD to study the internal hydration of BR solubilized in micelles of the nonionic detergent *n*-octyl- β -D-glucoside (OG). The monomeric BR micelles are found to be surprisingly stable and their rotational correlation time, obtained directly from the MRD

data, show that they are smaller than previously thought. Our results show that at least seven, and probably all ten, of the crystallographically identified internal water molecules in BR have residence times in the range 0.1–10 μ s at 4 °C. This result demonstrates that crystallographically well-defined water molecules in a membrane protein, despite being deeply buried and extensively H-bonded to the protein, exchange rapidly with water molecules in the external aqueous medium. Furthermore, these residence times provide important constraints on mechanistic models of proton translocation in BR.

Results

Methodological background

The theoretical basis and methodology of the MRD technique have been described in recent reviews.^{29,30} For convenience, we provide a brief summary here, which also serves to define the notation used in the subsequent analysis of the MRD data.

Magnetic relaxation dispersion refers to the dependence of the longitudinal (R_1) and transverse (R_2) relaxation rates on the resonance frequency ($\omega_0 = 2\pi \nu_0$), which is proportional to the applied static magnetic field. For the water ²H and ¹⁷O resonances, this dependence is of the form:

$$R_1 = 0.2J(\omega_0) + 0.8J(2\omega_0) \quad (1)$$

$$R_2 = 0.3J(0) + 0.5J(\omega_0) + 0.2J(2\omega_0) \quad (2)$$

The spectral density function (SDF) $J(\omega)$ is modeled as a constant α (up to the highest frequency investigated) plus a sum of Lorentzian terms, each characterized by an amplitude parameter β and a correlation time τ_C :

$$J(\omega) = \alpha + \sum_{k=1}^n \beta_k \tau_{Ck} [1 + (\omega \tau_{Ck})^2]^{-1} \quad (3)$$

Proton relaxation is induced by intramolecular and intermolecular dipole-dipole couplings. The intramolecular contribution is described by equations (1) and (2), but the intermolecular contribution involves a different linear combination of spectral density values.

Under the conditions of the present study, the magnetic relaxation rates depend on the strength of the nuclear electric quadrupole (²H and ¹⁷O) or magnetic dipole-dipole (¹H) coupling, given by the coupling frequency ω_Q or ω_D (which are known), and the correlation time τ_C , which essentially measures the rate of water rotation (see below). In the samples investigated here, the rate of water rotation varies by four orders of magnitude, depending on the location of the water molecule: from a few picoseconds in bulk water to tens of nanoseconds for internal water molecules that tumble rigidly with the protein. For this reason, a

single internal water molecule may contribute as much to the observed relaxation rates as 10^4 bulk water molecules.

In general, internal water molecules undergo fast local reorientation with respect to the protein. This "internal rotation", however, is usually highly anisotropic and therefore cannot average the quadrupole (or dipole) coupling to zero. Therefore, the spin relaxation rates are dominated by the much slower isotropic modulation of the coupling brought about by protein tumbling (correlation time τ_R) and/or water exchange to the bulk (water residence time τ_W). The fast "internal rotation" gives rise to a (usually negligible) direct relaxation contribution, subsumed in the α parameter in equation (1). More importantly, this "internal rotation" brings about a partial averaging of the anisotropic nuclear coupling so that only a part of it remains to be modulated by the slower protein tumbling and water exchange processes. This effect is described by the orientational order parameter S^2 , which scales the spectral density contribution associated with the slower motions (the β terms in equation (3)). The order parameter S^2 can vary from 0 for isotropic disorder to 1 for rigid binding (on the time-scale of τ_C).

In the following, we focus on the dependence of the observed relaxation rate on the mean residence time, τ_W , of the internal water molecules. (This discussion applies also to the case where the exchanging species is a proton or deuteron, rather than a water molecule.) The residence time affects the observed spin relaxation rate in two ways. First, the rate of orientational decorrelation, given by the inverse of the correlation time τ_C , is the sum of the protein tumbling rate ($1/\tau_R$) and the water exchange rate ($1/\tau_W$):

$$1/\tau_C = 1/\tau_R + 1/\tau_W \quad (4)$$

Unless $\tau_W \gg \tau_R$, the correlation time τ_C derived from the MRD data will therefore be shorter than τ_R . Second, the contribution of an internal water molecule to the observed relaxation rate is attenuated unless the exchange rate is much larger than the local magnetic relaxation rate, $R_1^{\text{loc}}(\omega_0) = \omega_Q^2 S^2 \tau_C \{0.2/[1 + (\omega_0 \tau_C)^2] + 0.8/[1 + (2\omega_0 \tau_C)^2]\}$. Because R_1^{loc} decreases with increasing frequency ω_0 , the fast-exchange condition $\tau_W R_1^{\text{loc}}(\omega_0) \ll 1$ will, in general, be more strongly violated at low frequencies. To satisfy the fast-exchange condition at all frequencies, we require that $\tau_W R^0 \ll 1$, where $R^0 = \omega_Q^2 S^2 \tau_C$ is the local zero-frequency relaxation rate. Outside the fast-exchange regime, the observed relaxation rate R_1 will be more suppressed at low frequencies than at high frequencies. This also has the effect of shifting the dispersion curve $R_1(\nu_0)$ to higher frequencies. To a very good approximation, both the attenuation and the frequency shift can be described by the fast-exchange equations (1) to (3), provided that α , β , and τ_C are replaced by the corresponding renormalized parameters α' , β' , and τ_C' (see below).

The sum over k in equation (3) represents the contributions to the relaxation dispersion from water molecules with different correlation times τ_{Ck} . Although the individual internal water molecules in a protein (such as BR) experience the same global tumbling time τ_R , they will, in general, have different residence times τ_{Wk} and therefore different correlation times τ_{Ck} (cf. equation (4)). However, as long as $\tau_{Wk} \gg \tau_R$, this dynamic heterogeneity is not manifest and the observed dispersion yields the same correlation time, $\tau_C = \tau_R$, for all such water molecules.

In the fast-exchange regime ($R^0 \tau_W \ll 1$), the interpretation of the SDF parameters in equation (3) is straight-forward.^{29,30} From the amplitude parameter β_k we obtain $N_k S_k^2 = N_T \beta_k / \omega_Q^2$, where N_k is the number of water molecules with correlation time τ_{Ck} and N_T is the total number of water molecules (obtained from the protein concentration), both counted per protein molecule. Since the orientational order parameter is expected to vary among different internal hydration sites, the S_k^2 value deduced from the β_k parameter is an average over the N_k water molecules.

Even outside the fast-exchange regime, the relaxation rates can be described by an SDF of the same functional form as in equation (3), but with renormalized parameters α' , β'_k , and τ_{Ck}' . The relation between these renormalized parameters and the true parameters α , β_k , and τ_{Ck} is different for R_1 and R_2 (see Materials and Methods). Therefore, if both R_1 and R_2 have been measured, a deviation from the fast-exchange limit can be diagnosed from the shape of the dispersion profiles and a joint fit yields the additional parameter $\tau_{Wk} S_k^2$. As seen from the relations between the renormalized parameters β'_k and τ_{Ck}' and the true parameters β_k and τ_{Ck} (see Materials and Methods), information about the residence time τ_{Wk} can be obtained even when $\tau_{Wk} \gg \tau_R$ and, according to equation (4), $\tau_C = \tau_R$. This is possible because when the fast-exchange condition $R^0 \tau_W \ll 1$ is violated, i.e. when the water residence time is no longer short compared to the local spin relaxation time (here, ca 20 μs for ^2H and 0.3 μs for ^{17}O at 4°C), both the amplitude and the frequency of the dispersion step are reduced as compared to the fast-exchange situation (cf. equation (7)).

MRD measurements were carried out on aqueous solutions of BR solubilized in micelles of the nonionic detergent OG. Sample compositions are given in Table 1.

Size of detergent micelles containing BR

MRD data provide information about hydration and about the size and shape of the BR-loaded detergent micelles *via* their rotational correlation time τ_R . If the micelle is modeled as a smooth rigid sphere of volume V immersed in a solvent of viscosity η , then the rank-2 rotational correlation time probed by MRD is given by:

Table 1. Samples investigated by MRD

Sample	[BR] (mM)	[OG] (mM)	pH* ^{a,b}	x_2^c	x_{17}^d	t (°C)	Isotope
A1	0.53	135	4.6	0.998	h	4	² H
A2 ^e	0.46	118	4.7	0.873	0.044	4	¹⁷ O
B	0.64	g	5.0	0.686	0.110	27	¹⁷ O
C1	0.96	g	4.9	0.998	h	27	² H
C2 ^f	0.79	g	4.9	0.998	h	27	¹ H
D1	0	120	4.7, 10.7	0.998	h	4, 27	² H
D2	0	120	4.7	0.746	0.089	4	¹⁷ O

^a pH* was measured with an electrode calibrated in H₂O buffers and is related to the thermodynamic L₃O⁺ (L = H or ²H) ion activity through $pL = pH^* + 0.41 x_2$.

^b All samples contained 5 mM acetate buffer.

^c Atom fraction ²H in water.

^d Atom fraction ¹⁷O in water.

^e Sample A2 was obtained by diluting sample A1 with ¹⁷O-enriched H₂O.

^f Sample C2 is the supernatant obtained after centrifuging sample C1.

^g Not determined, but probably similar to samples A1 and A2.

^h Natural abundance, $x_{17} = 0.00037$.

$$\tau_R = \eta V / (k_B T) \quad (5)$$

Although BR forms a trimer in the purple membrane, the correlation times derived from our MRD data show that the micelle contains only one BR molecule (see below). This is in accordance with the results of previous circular dichroism and gel-filtration studies.^{23,24} We can therefore write $V = V_{BR} + N_{OG} V_{OG}$, where V_{BR} and V_{OG} are the molecular volumes of BR and OG, and N_{OG} is the number of OG molecules in the micelle. Using the molar mass of BR, 27 kg mol⁻¹, and an estimated partial specific volume of 0.75 cm³ g⁻¹, we obtain a protein volume of $3.36 \times 10^4 \text{ \AA}^3$. Adding 250 water molecules estimated to be in direct contact with the solvent-exposed surfaces of BR (see below), we get $V_{BR} = 4.1 \times 10^4 \text{ \AA}^3$. For OG,³² the molar mass of 292.4 g mol⁻¹ and the partial specific volume 0.867 cm³ g⁻¹ yield a molecular volume of 420 \AA^3 , to which we add six water molecules hydrating the glucose head group, giving $V_{OG} = 600 \text{ \AA}^3$. (The rationale for adding a layer of hydration water is essentially empirical and may actually compensate more for surface roughness than for solvent perturbation.)

Figure 1 shows the rotational correlation time obtained with these volumes and with the bulk water viscosity at 4 and 27 °C (at the isotope compositions of samples A2 and B in Table 1). Since the micelle cannot be perfectly spherical, the real τ_R should be slightly longer than predicted by Figure 1. Any residual native lipids will also increase τ_R .

The overall OG/BR (mol/mol) ratio was determined to be 256 in samples A1 and A2 (see Materials and Methods), and is probably not very different in the other BR samples. These 256 OG molecules are divided among BR-loaded micelles (N_{OG} molecules), BR-free micelles, and monomers. The critical micelle concentration (cmc) of OG varies from 25 mM at 27 °C to 35 mM at 4 °C,³² corresponding to about 75 monomeric OG molecules per BR molecule in sample A2. Using the geometry

of the BR molecule together with the 243 \AA^3 alkyl chain volume³³ and 44 \AA^2 head group area of OG,³⁴ we estimate that N_{OG} is in the range 75-150. In the absence of BR, OG forms micelles with an aggregation number of ca 90 and a moderately non-spherical shape.^{32,34,35}

In principle, τ_R can be obtained directly from the dispersion of the non-labile protons of BR, for which $\tau_C = \tau_R$ by definition. However, with a zero-frequency relaxation time of the order of 1 ms, these protons cannot be studied quantitatively by

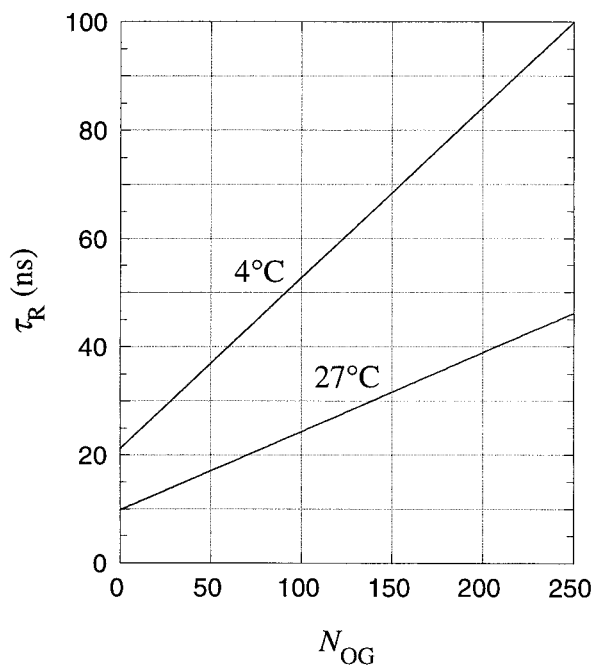


Figure 1. Theoretical estimate of the rotational correlation time, τ_R , of a micelle containing one BR molecule and N_{OG} OG molecules along with a layer of hydration water. The micelle is modeled as a smooth sphere immersed in a fluid with the viscosity of bulk water at 4 °C (2.00 cP) or 27 °C (1.00 cP) and the isotope composition of samples A2 and B.

field-cycling MRD (see Materials and Methods). The situation is more favorable for the non-labile protons of OG, which relax one to two orders of magnitude slower than the BR protons because of their smaller order parameter (due to fast rotational isomerization in the alkyl chain and, to a lesser extent, to lateral diffusion of OG molecules over curved interfaces) and because of exchange-averaging with monomeric OG molecules and BR-free micelles (which have considerably shorter τ_R than BR-loaded micelles). The residence time of OG molecules in micelles is about 1 μ s.³⁵ This is much shorter than the local spin relaxation time, but much longer than the tumbling time. Consequently, we have $\tau_C = \tau_R$ for non-labile OG protons.

Although the total ^1H signal should relax multi-exponentially, the observed relaxation is exponential within experimental error. This is because the non-labile BR protons (ca 40% of the initial ^1H signal) relax too rapidly to contribute to the acquired signal, whereas the labile protons originating from the hydroxyl groups in OG (<10% of the initial ^1H signal) have a zero-frequency relaxation rate of ca 1 s^{-1} (as verified by direct MRD measurements on a sample prepared with a $\text{H}_2\text{O}/^2\text{H}_2\text{O}$ mixture), thereby making a negligible contribution to the observed relaxation. Finally, the spread of R_1 values among different OG protons due to the order parameter gradient along the alkyl chain is too small to be resolved.

Figure 2 shows the ^1H R_1 dispersion from sample C2, made with $^2\text{H}_2\text{O}$. The bi-Lorentzian fit shown yields for the longer correlation times 35(\pm 3) ns, which must be the tumbling time of BR-loaded micelles. According to equation (5), $\tau_R = 35$ ns corresponds to an apparent Stokes radius of 32 \AA , comparable to previous gel-filtration results.^{23,24} According to Figure 1, $\tau_R = 35$ ns corresponds (after a viscosity scaling from 1.04 to 1.00 cP) to an OG aggregation number $N_{\text{OG}} = 165$, or somewhat less if the non-spherical shape of the micelle and/or some residual lipid is taken into account. This result is not inconsistent with our geometrically based N_{OG} estimate (see above).

The shorter correlation time of 2.9(\pm 0.4) ns obtained from the bi-Lorentzian fit in Figure 2 can be attributed to tumbling of BR-free micelles and to lateral diffusion of OG molecules over the curved interfaces of both types of micelle, processes that are expected to have correlation times of a few nanoseconds. The amplitude parameter $\beta = (\omega_D S)^2$ associated with the long correlation time is 3.8(\pm 0.3) $\times 10^8 \text{ s}^{-2}$. With a dipole-dipole coupling frequency ω_D of 1.64 $\times 10^5 \text{ rad s}^{-1}$, as expected for a CH_2 group with $r_{\text{HH}} = 1.78 \text{ \AA}$, we obtain the reasonable order parameter $S = 0.12$.³⁶

Stability of detergent-solubilized BR

The samples that were kept at 27°C during measurements (several days) showed evidence (from light-scattering) of a slow aggregation pro-

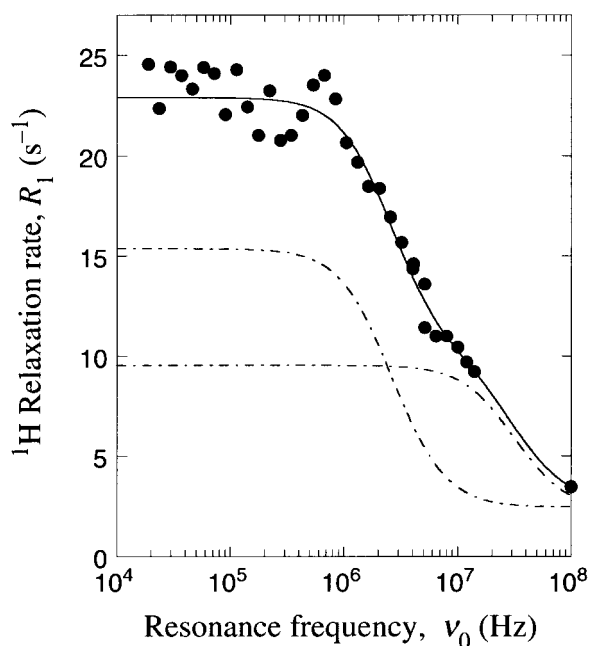


Figure 2. Frequency-dependence of the longitudinal relaxation rate of the non-labile OG protons in an aqueous solution of BR solubilized in OG micelles (sample C2) at 27°C. The continuous curve resulted from a fit to the R_1 data using a bi-Lorentzian SDF. The dash-dot curves represent the individual Lorentzian R_1 components.

cess, leading to visible precipitation after about a week at this temperature. The presence of higher aggregates during the MRD measurements at 27°C was also inferred from a large step at sub-MHz frequencies in the ^1H and ^2H dispersions.

This is illustrated in Figure 3, showing the ^2H R_1 dispersion from sample C1 at 27°C. The dominant dispersion step at sub-MHz frequencies is attributed to labile OG deuterons in the large micelles (see below). Fixing τ_{C1} and τ_{C2} at the values obtained from the ^{17}O MRD data at this temperature (see below), a tri-Lorentzian fit yields $\tau_{\text{C3}} = 0.9(\pm 0.1) \mu\text{s}$ for the third correlation time. For such long correlation times, the conventional perturbation theory of spin relaxation, on which our analysis is based, breaks down and τ'_{C3} is therefore only an apparent correlation time (hence the prime) related to the true correlation time through $\tau'_{\text{C3}} = \tau_{\text{C3}} (1 + \Omega_Q \tau_{\text{C3}})^{-1/2}$, where $\Omega_Q = (3/2)^{1/2} \omega_Q S$.³⁷ In the limit $\Omega_Q \tau_{\text{C3}} \gg 1$, we have $\tau'_{\text{C3}} = 1/\Omega_Q$, which equals 3 μs for the OD deuterons in OG. The observed value of τ'_{C3} indicates that we are close to this limit. The correlation time τ_{C3} could be the tumbling time of the aggregates, or, more likely, the residence time of an OG molecule in the aggregate, which is about 1 μs .³⁵ In the latter case, equation (3) implies that $\tau_R \gg 1 \mu\text{s}$. The exchange of OG molecules is thus three orders of magnitude faster than the exchange of their OD

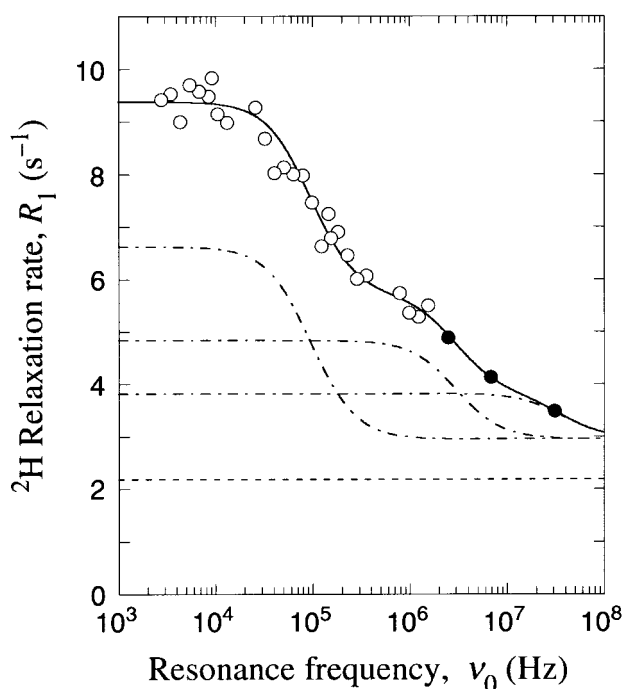


Figure 3. Frequency-dependence of the water ^2H longitudinal relaxation rate in an aqueous solution of BR solubilized in OG micelles (sample C1) at 27°C . Open circles represent R_1 values measured with the FC technique. The broken line refers to the relaxation rate of the bulk water used in this sample. The continuous curve resulted from a tri-Lorentzian SDF with τ_{C1} and τ_{C2} frozen at values derived from the ^{17}O MRD data at 27°C (see Table 2). The dash-dot curves represent the individual Lorentzian R_1 components.

deuterons (about 2 ms at 27°C , see below). Even the lower bound of ca 1 μs for τ_{R} is much larger than the expected tumbling time of a detergent-solubilized BR trimer, which should be roughly three times that of a monomeric BR micelle, that is, ca 100 ns at 27°C .

Because of partial overlap with the very large sub-MHz dispersion step from the higher aggregates and because of the uncertainty in the amount of non-aggregated BR, a quantitative analysis of the more extensive ^2H MRD data recorded on sample B in the 1-100 MHz range (data not shown) could not yield unambiguous information about BR hydration. It should also be noted that the ^1H dispersion in Figure 2, which does not exhibit the low-frequency dispersion step seen in Figure 3, was recorded within two days after the higher aggregates had been removed from the solution by centrifugation.

In contrast to the samples that were measured at 27°C (but stored at 4°C), the samples that were measured (and stored) at 4°C remained stable for at least eight months. Figure 4 shows the UV/VIS absorption spectra of OG-solubilized BR from one of the three BR preparations used for the MRD

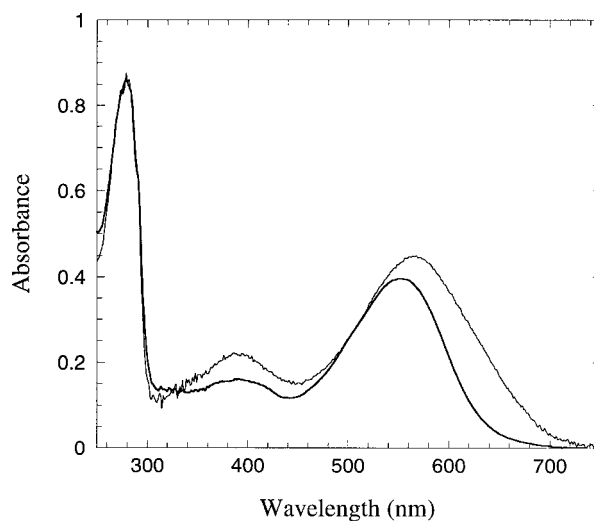


Figure 4. UV/VIS absorption spectra from aqueous solutions ($\text{pH}^* 4.7$) of BR solubilized in OG micelles, recorded immediately after preparation of the stock solution (thick line) or after eight months storage at 4°C (sample A2 diluted tenfold with H_2O) (thin line). The spectra have been normalized in amplitude at 280 nm.

work (see Table 1 and Materials and Methods). The spectrum obtained from sample A2 after eight months does not differ much from the spectrum recorded immediately after preparation of the stock solution, indicating that the protein remains essentially in a native state. The observable differences, a 10 nm red shift and asymmetric broadening of the bound-retinal band around 560 nm and a slightly increased intensity of the 390 nm band, may be ascribed to minor structural or charge alterations in the vicinity of the chromophore, as observed in mutant forms of BR.³⁸ The slight variation of the 280/560 nm absorbance ratio is partly due to concentration-dependent light-scattering. The spectrum (not shown) recorded in connection with the MRD measurements, ca three months after preparation of the stock solution, was virtually identical with the eight month spectrum shown in Figure 4. Consistent with these spectral indications of little or no "bleaching" over several months when the sample was kept in the dark at 4°C and $\text{pH}^* 4.7$, no sub-MHz dispersion step was seen at 4°C .

^2H MRD studies of deuterium exchange in OG

The relaxation of the water ^2H resonance usually includes contributions from rapidly exchanging labile deuterons.^{29,30} Any such contributions must be assessed before information about protein hydration can be extracted from ^2H MRD data. In the samples studied here, the protein is not the only source of labile deuterons; the glucose head group of the detergent contains four labile hydroxyl deuterons. To assess this potentially

important contribution, a reliable value for the hydroxyl deuteron residence time, τ_{OD} , is needed. To this end, we measured the ^2H R_1 and R_2 dispersions from a 120 mM OG solution in $^2\text{H}_2\text{O}$ (sample D1) at pH^* 4.7 (as in the BR solution) and at pH^* 10.7 (where the hydroxyl deuterons are in the fast-exchange regime). This was done at 4 °C and at 27 °C, but the 27 °C dispersions were too small to permit a quantitative analysis. Although consistent with the R_1 data, the R_2 data showed more scatter and were therefore not included in the analysis.

The ^2H R_1 dispersions from sample D1 at 4 °C and at two pH^* values are shown in Figure 5. Because the hydration water of OG has sub-nanosecond residence times (as evidenced by the lack of ^{17}O dispersion; see below), these dispersions are entirely due to labile OG deuterons. As expected, each dispersion is well described by a Lorentzian SDF. Rather than fitting the two dispersions separately, which would require six parameters, they were fitted jointly with two constraints imposed, leaving four free parameters. Let α , β , and τ_c be the parameters of the pH^* 10.7 dispersion, where the hydroxyl deuterons are in the fast-exchange regime. Then the parameters at pH^* 4.7 are $\alpha' = \alpha$, $\beta' = \beta(1 + R^0 \tau_{OD})^{-1/2}$, and $\tau_c' = \tau_c(1 + R^0 \tau_{OD})^{-1/2}$, where R^0 is the zero-frequency relaxation rate of the hydroxyl deuterons (see Materials and Methods). Because only the pH^* value is different,

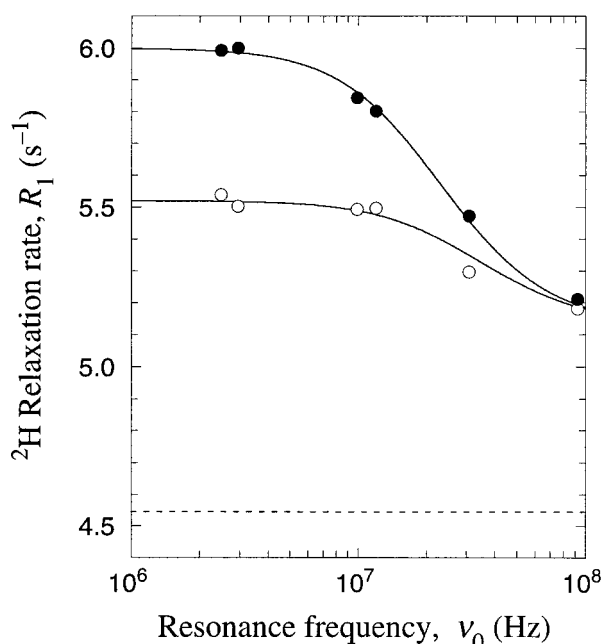


Figure 5. Frequency-dependence of the water ^2H longitudinal relaxation rate in an aqueous solution of OG (sample D1) at 4 °C and at pH^* 4.7 (open circles) or pH^* 10.7 (filled circles). The broken line refers to the relaxation rate of the bulk water used in these samples. The continuous curves resulted from a joint Lorentzian fit to the two sets of R_1 data with the constraint that only the residence time of the OG hydroxyl deuterons is affected by the pH^* difference.

all parameters should be the same for the two dispersions except τ_{OD} . At pH^* 10.7, $R^0 \tau_{OD} \ll 1$, but this fast-exchange condition is not satisfied at pH^* 4.7. To obtain τ_{OD} , we note that $R^0 = b \tau_c$ and $\beta = x f_{OD} b$. Here $b = (3\pi^2/2) (\chi_{OD} S_{OD})^2$, x is the fraction of micellized OG molecules, and f_{OD} is the fraction of all deuterons that reside in the hydroxyl groups of OG. Since $R^0 = \beta \tau_c / (x f_{OD})$, we can deduce τ_{OD} from the fit if we know x and f_{OD} . With a cmc of 35 mM at 4 °C,³² $x = 1 - 35/120 = 0.71$. Furthermore, for 120 mM OG in $^2\text{H}_2\text{O}$, $f_{OD} = 4 [\text{OG}]/(2 [^2\text{H}_2\text{O}]) = 4.47 \times 10^{-3}$. From the values of $R^0 \tau_{OD}$, β and τ_c derived from the fit, we thus obtain $\tau_{OD} = 4.5(\pm 0.4)$ ms. This is consistent with the previously determined hydroxyl deuteron residence time of 2 ms in glucose at 20 °C and pH^* 6-7.³⁹ The correlation time, $\tau_c = 3.9(\pm 0.1)$ ns, may be attributed to the combined effect of micelle tumbling and lateral diffusion of OG molecules over the curved micelle surface.⁴⁰ The quadrupole coupling constant χ_{OD} for the hydroxyl deuterons in OG should fall within the range 190-210 kHz determined for simple alcohols.^{41,42} With this value and the β value determined from the fit, we obtain an order parameter, $S_{OD} = 0.35 \pm 0.02$, in the expected range.

^2H MRD studies of BR hydration

If care is taken to eliminate or correct for any contribution from labile deuterons, ^2H MRD offers certain advantages over ^{17}O MRD in hydration studies. Because of the one order of magnitude weaker quadrupole coupling, ^2H relaxation is two orders of magnitude slower than ^{17}O relaxation. This makes it possible to use the field cycling (FC) technique to access the kHz-MHz frequency range (see Materials and Methods). Large aggregates can thereby be identified directly *via* their associated low-frequency dispersion (see Figure 3), rather than merely *via* an R_2 offset (see below). Moreover, because of the longer relaxation times, ^2H MRD can reveal the presence of internal water molecules that exchange too slowly to contribute to ^{17}O relaxation.

The ^2H MRD data obtained at 4 °C (from sample A1) are shown in Figure 6. Despite the scatter in the low-frequency FC data, it is clear that R_1 levels out and converges with R_2 at about 0.2 MHz, demonstrating the absence of larger aggregates (as seen at 27 °C). Because we could not rule out a minor contribution to R_2 at the higher frequencies from chemical shift modulation by exchange of labile deuterons,²⁹ only the R_1 data were included in the quantitative analysis. The parameter values obtained from a bi-Lorentzian fit to the R_1 data are given in Table 2. We focus on the low-frequency step with correlation time τ_{c1} . Before drawing any conclusions from the parameter values characterizing this dispersion step, we must ascertain whether they are affected by labile deuterons.

On the basis of the amino acid composition of BR and typical labile deuteron exchange rate con-

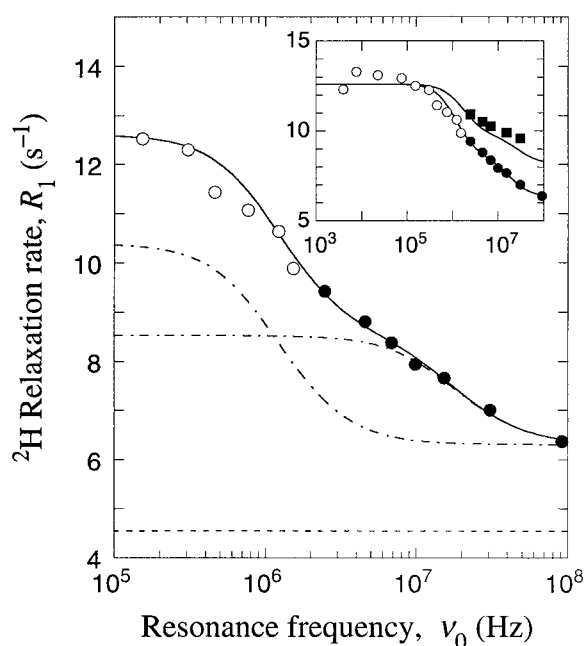


Figure 6. Frequency-dependence of the water ^2H longitudinal (circles) and transverse (filled squares) relaxation rates in an aqueous solution of BR solubilized in OG micelles (sample A1) at 4°C . Open circles represent R_1 values measured with the FC technique. The broken line refers to the relaxation rate of the bulk water used in this sample. The continuous curve resulted from a fit to the R_1 data using a bi-Lorentzian SDF with parameter values given in Table 2. The dash-dot curves represent the individual Lorentzian R_1 components. The inset shows R_1 data over a wider frequency range and includes R_2 data along with the R_2 dispersion predicted on the basis of the parameter values obtained from the fit to the R_1 data.

starts,⁴³ we estimate the contribution of labile BR deuterons to the zero-frequency ^2H relaxation rate at $\text{pH}^* 4.7$ and 4°C to be less than 0.3 s^{-1} . This contribution can therefore be neglected. The contribution from labile OG deuterons can be estimated with the aid of the values of τ_{OD} , χ_{OD} , and S_{OD} established above. Taking $\tau_{\text{R}} = 72 \text{ ns}$ (see below), we obtain for the zero-frequency relaxation contribution from labile deuterons in N_{OG} OG molecules

per aggregate, $\Delta R_1(0) = (2 N_{\text{OG}} / N_{\text{T}}) b \tau_{\text{R}} / (1 + b \tau_{\text{R}} \tau_{\text{OD}}) = 4 \times 10^{-3} N_{\text{OG}} \text{ s}^{-1}$. For a plausible aggregation number, $N_{\text{OG}} = 150$, this amounts to 0.6 s^{-1} , or 15% of the low-frequency dispersion step in Figure 6. This is likely to be an overestimate, since S_{OD} should be further reduced by lateral diffusion of OG molecules over the curved micelle surface. We therefore neglect the OG contribution to the ^2H dispersion at 4°C .

Having demonstrated that the labile deuteron contributions are negligible, we may now conclude from the amplitude parameter $N_1 S_1^2 = 7.7 \pm 1.0$ that BR contains at least seven long-lived water molecules (since $S_1^2 \leq 1$). The correlation time, $\tau_{\text{C1}} = 72(\pm 8) \text{ ns}$, allows us to quantify the meaning of long-lived. First, according to equation (4), the residence time must be longer than the correlation time, $\tau_{\text{W1}} > \tau_{\text{C1}}$. Second, for a water molecule to contribute fully to the dispersion, its residence time must be shorter than the local zero-frequency relaxation time, $\tau_{\text{W1}} < 1/(\omega_{\text{Q}}^2 S_1^2 \tau_{\text{C1}})$ (see Materials and Methods). Using the known value²⁹ of ω_{Q} and setting $S_1 = 1$ (only for the purpose of estimating the upper bound on τ_{W1}), we can thus say that the seven or more water molecules responsible for low-frequency ^2H dispersion have residence times in the range $70 \text{ ns} < \tau_{\text{W1}} < 20 \mu\text{s}$. Furthermore, the correlation time $\tau_{\text{C1}} = 72 \text{ ns}$ can be identified with the tumbling time, τ_{R} , of a BR-loaded micelle at 4°C , since it agrees, after viscosity scaling (the bulk water viscosity ratio is 1.98), with the value, $\tau_{\text{R}} = 35 \text{ ns}$, obtained from the non-labile proton dispersion at 27°C (see Figure 2).

^{17}O MRD studies of BR hydration

The main objective of this work is to determine the number of internal water molecules in BR and their residence times. This is accomplished most directly by ^{17}O MRD, which reports exclusively on water molecules. Because of the fast spin relaxation of the ^{17}O nucleus, however, we cannot use the field-cycling technique to access sub-MHz frequencies, as required to sample the entire dispersion curve for the relatively long correlation times involved here. We compensate for this limitation by also measuring the transverse relaxation rate R_2 , which includes zero-frequency information at

Table 2. Results derived from bi-Lorentzian fits to ^2H and ^{17}O MRD data

Isotope/sample Temperature ($^\circ\text{C}$)	$^2\text{H}/\text{A1}$ 4	$^{17}\text{O}/\text{A2}$ 4	$^{17}\text{O}/\text{B}$ 27
α (s^{-1})	6.3 ± 0.1	400 ± 4	171 ± 2
$N_1 S_1^2$ ^a	7.7 ± 1.0	4.9 ± 0.4	4.2 ± 0.4
τ_{C1} (ns)	72 ± 8	61 ± 5	30 ± 5
$N_2 S_2^2$ ^a	61 ± 6	20 ± 4	10 ± 2
τ_{C2} (ns)	5.0 ± 0.6	3.6 ± 0.7	2.4 ± 0.5
ΔR_2 (s^{-1})	-	-	29 ± 3

For the ^{17}O MRD data, R_1 and R_2 were fitted jointly. Parameter errors are Monte Carlo estimates (\pm one standard deviation) based on experimental errors in R_1 and R_2 (1-2%).

^a The β_k parameters were converted to $N_k S_k^2$ using $\omega_{\text{Q}}(^{17}\text{O}) = 7.6 \times 10^6 \text{ rad s}^{-1}$ and $\omega_{\text{Q}}(^2\text{H}) = 8.7 \times 10^5 \text{ rad s}^{-1}$.

all resonance frequencies *via* the first term in equation (2).

The ^{17}O MRD data obtained at 4°C (from sample A2) and at 27°C (from sample B) are shown in Figures 7 and 8. In both cases, the dispersion curves shown resulted from a joint fit to the combined R_1 and R_2 data using a bi-Lorentzian SDF. (A uni-Lorentzian SDF was ruled out.) The parameter values derived from these fits are collected in Table 2. At 27°C , a fraction of the BR molecules are present in larger aggregates that give rise to a sub-MHz dispersion step (see above). This dispersion step, which is observed directly in the ^2H data (see Figure 3), is much smaller for ^{17}O (since only water molecules contribute) and, therefore, does not affect R_1 above 1 MHz, and only adds a frequency-independent contribution to R_2 *via* the term $0.3 J(0)$ in equation (2). We therefore included an R_2 offset, ΔR_2 , in the fit to the 27°C ^{17}O data. To allow a more direct comparison with the 4°C data in Figure 7, the ΔR_2 value resulting from the fit was subsequently subtracted from the R_2 dispersion curve as well as from the R_2 data shown in Figure 8.

The dominant dispersion step, with correlation time τ_{C1} , is well characterized by the combined R_1 and R_2 data. (Recall that R_2 contains information

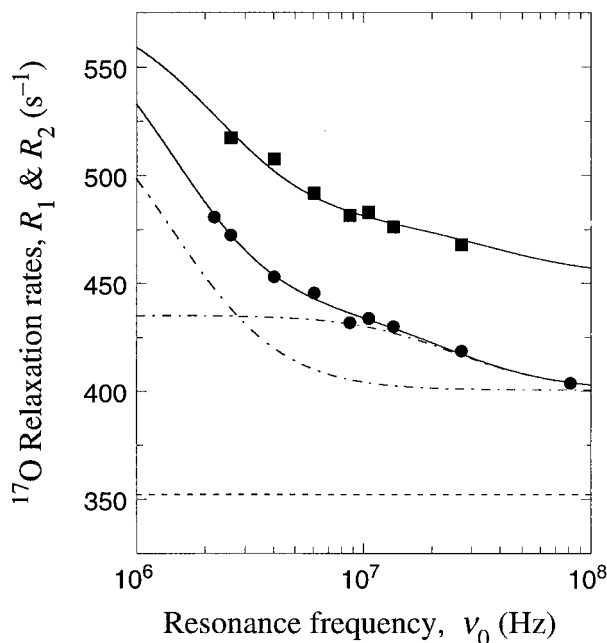


Figure 7. Frequency-dependence of the water ^{17}O longitudinal (circles) and transverse (squares) relaxation rates in an aqueous solution of BR solubilized in OG micelles (sample A2) at 4°C . The broken line refers to the relaxation rate of the bulk water used in this sample. The continuous curves resulted from a joint fit to the combined R_1 and R_2 data using a bi-Lorentzian SDF with parameter values given in Table 2. The dash-dot curves represent the individual Lorentzian R_1 components.

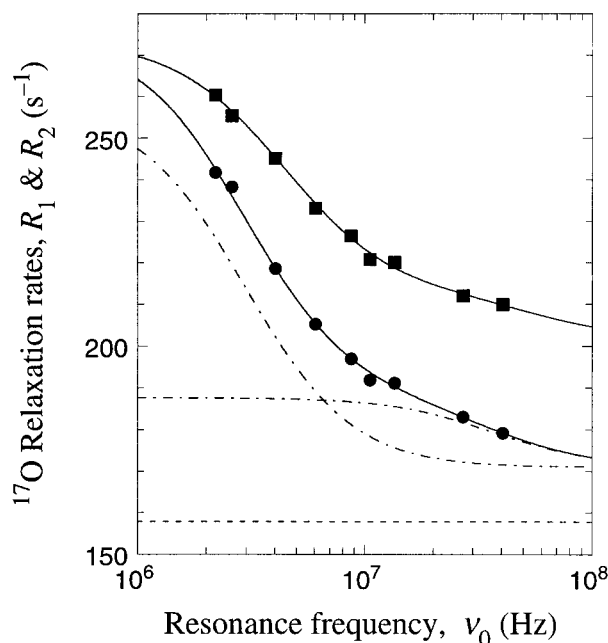


Figure 8. Frequency-dependence of the water ^{17}O longitudinal (circles) and transverse (squares) relaxation rates in an aqueous solution of BR solubilized in OG micelles (sample B) at 27°C . The broken line refers to the relaxation rate of the bulk water used in this sample. The curves resulted from a joint fit to the combined R_1 and R_2 data, using a bi-Lorentzian SDF with parameter values given in Table 2. A frequency-independent R_2 offset of 29.2 s^{-1} has been subtracted from the R_2 data and dispersion curve (see the text). The dash-dot curves represent the individual Lorentzian R_1 components.

about the low-frequency plateau.) Because water molecules associated with detergents or lipids (in micelles or liquid crystals) or with protein surfaces invariably have sub-nanosecond residence times,⁴⁴ this dispersion step must be due to water molecules trapped in cavities within the BR molecule. (The absence of long-lived OG hydration was confirmed by the finding that $R_1 = R_2$ within experimental error for the ^{17}O relaxation from sample D2, containing 120 mM OG but no protein.) The ^{17}O parameter values obtained at 4°C , $N_1 S_1^2 = 4.9 \pm 0.4$ and $\tau_{\text{C1}} = 61(\pm 5)$ ns, imply that BR contains at least five water molecules (since $S_1^2 \leq 1$) with a residence time $\tau_{\text{W1}} > 60$ ns (since $\tau_{\text{W1}} > \tau_{\text{C1}}$). The barely significant reduction of $N_1 S_1^2$ at 27°C (see Table 2) may be explained by the presence of a fraction ϕ of the BR in the form of larger aggregates (responsible for the R_2 offset); the number given in Table 2 is then $(1 - \phi) N_1 S_1^2$.

The ^{17}O MRD data yield for the correlation time of the dominant dispersion step $\tau_{\text{C1}} = 61(\pm 5)$ ns at 4°C and $30(\pm 5)$ ns at 27°C . Because these correlation times (ratio 2.03) scale as the bulk water viscosity at the two temperatures (ratio 2.01), equation (4) suggests that $\tau_{\text{C1}} \approx \tau_{\text{R}}$, the tumbling time of a BR-loaded micelle. (Had the residence

τ_{W1} been comparable to or shorter than τ_R , then its supposedly stronger temperature-dependence would have been partly carried over to τ_{C1} .) On the other hand, the ^{17}O correlation times are both 15% shorter than the tumbling times, τ_R , derived from the ^1H and ^2H dispersions (see above). This indicates that the water molecules that are responsible for the ^{17}O dispersions have residence times that are not very much longer than τ_R . With $\tau_R = 72$ ns from the 4°C ^2H dispersion, the ^{17}O correlation time implies, *via* equation (4), residence times in the range 300-400 ns at 4°C . With residence times in this range, the fast-exchange condition is not likely to be satisfied; the local zero-frequency ^{17}O relaxation time of a fully ordered water molecule with $\tau_C = 60$ ns is merely ca 300 ns. We therefore cannot assume that fast-exchange conditions prevail for the ^{17}O relaxation.

To allow for the possibility that the internal water molecules are not fully in the fast-exchange limit, an additional parameter, chosen as $\tau_{W1} S_1^2$, must be introduced. Because the accuracy of the data does not allow us to determine this parameter directly, we fitted the other parameters for different fixed values of $\tau_{W1} S_1^2$. Fits of acceptable quality were obtained with $\tau_{W1} S_1^2 = 200$ ns (at either temperature). For example, for $\tau_{W1} S_1^2 = 200$ ns, we obtained $\tau_{C1} = 57$ ns and $N_1 S_1^2 = 7.0$ at 4°C . With $\tau_R = 70$ ns (as suggested by the ^1H and ^2H MRD data), we then get $\tau_{W1} = 300$ ns, $S_1 = 0.8$, and $N_1 = 10.7$. (This analysis ignores the slight complication introduced by a distribution of residence times for the internal water molecules that contribute to the dispersion step.) In conclusion, the ^{17}O MRD data identify internal water molecules in BR, the number (N_1), order parameter (S_1), and residence time (τ_{W1}) of which are such that $N_1 S_1^2 = 5-7$, $\tau_{W1} > 60$ ns, and $\tau_{W1} S_1^2 \leq 200$ ns (at 4°C). Although the data do not set a lower bound on the order parameter, previous MRD studies of internal water molecules in proteins suggest that $S^2 \geq 0.5$ for water molecules that participate in at least two H bonds,^{45,46} which is the case for all the seven crystallographically identified water molecules in the EC channel.

On the other hand, the ^2H MRD data showed that $N_1 S_1^2 = 7.7 \pm 1.0$ and 70 ns $< \tau_{W1} < 20$ μs at 4°C . The question now arises of whether the ^2H dispersion can be fully accounted for by the water molecules that produce the ^{17}O dispersion, or if we need to invoke an additional ^2H contribution from water molecules that exchange too slowly to contribute to ^{17}O relaxation. To answer this question, we must recognize that, because of geometrical differences between the ^2H and ^{17}O quadrupole coupling tensors, the order parameters $S(^2\text{H})$ and $S(^{17}\text{O})$ may differ.²⁹ We tentatively divide the water molecules responsible for the ^2H dispersion in two groups: "fast" water molecules with $\tau_{W1f} < 0.5$ μs that also contribute to the ^{17}O dispersion, and "slow" water molecules, with $2 < \tau_{W1s} < 20$ μs , that contribute only to the ^2H dispersion. Since the correlation times of the ^{17}O and

^2H dispersions differ by only ca 20%, the contributions to $N_1 [S_1(^2\text{H})]^2$ from the "fast" and "slow" water molecules are approximately additive. We can therefore write:

$$N_1 [S_1(^2\text{H})]^2 = N_{1s} [S_{1s}(^2\text{H})]^2 + \sigma N_{1f} [S_{1f}(^{17}\text{O})]^2 \quad (6)$$

where $\sigma = [S_{1f}(^2\text{H})/S_{1f}(^{17}\text{O})]^2$. For physically realistic situations, σ ranges from 1 for a fully ordered water molecule to 0.37 for a water molecule that flips around the C_2 symmetry axis on a time-scale less than τ_{C1} but is otherwise highly ordered.²⁹ The relationship (6) is illustrated graphically in Figure 9, showing that the MRD data are consistent with $N_{1s} [S_{1s}(^2\text{H})]^2$ values in the range 1-6, with larger values corresponding to rapidly flipping "fast" water molecules.

^{17}O MRD evidence for faster motions

A high-frequency dispersion step, with a correlation time of a few nanoseconds (see Table 2), is evident in Figures 7 and 8 (as well as in the ^2H dispersion of Figure 6). If the water molecules responsible for this dispersion step are associated with the BR-loaded micelle, then they must have residence times of a few nanoseconds ($\tau_{W2} = \tau_{C2} \ll \tau_R$). Although water molecules in deep surface pockets on protein surfaces have been found to have residence times in this range, the large value of $N_2 S_2^2$ (see Table 2) is difficult to rationalize in this way.

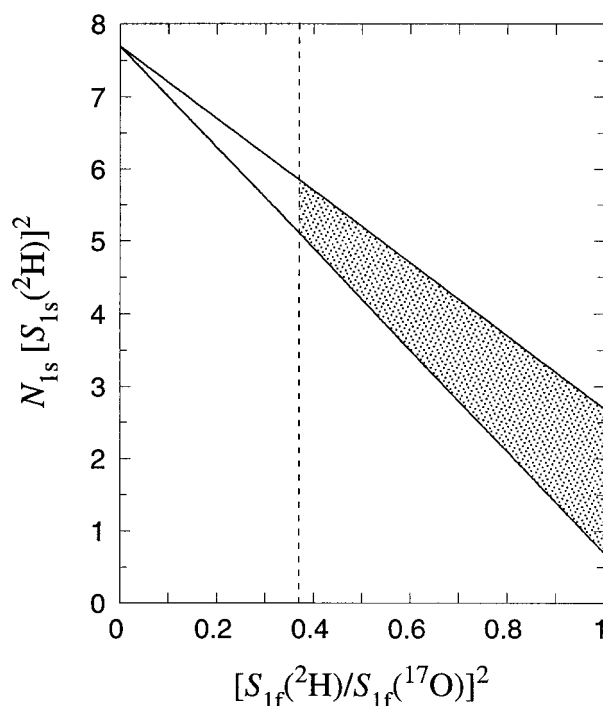


Figure 9. Graphical representation of equation (6). The possible values for $N_{1s} [S_{1s}(^2\text{H})]^2$ are confined to the shaded region, bounded from above and below by the experimental result $5 \leq N_{1f} [S_{1f}(^{17}\text{O})]^2 \leq 7$, and from left and right by the condition $0.37 \leq [S_{1f}(^2\text{H})/S_{1f}(^{17}\text{O})]^2 \leq 1$.

Another possibility would be to assign this dispersion step to the primary hydration of two or three BR-bound calcium or magnesium ions. In the case of Ca^{2+} , $\tau_{\text{C}2}$ could be the residence of water molecules in the ionic hydration shell, whereas, for Mg^{2+} , the hydration is much more long-lived, so $\tau_{\text{C}2}$ would have to be the residence time of the ion. Although BR in purple membrane is known to bind Ca^{2+} or Mg^{2+} ,^{47,48} no such ions have been localized in X-ray crystal structures of BR. Yet another possibility is that a substantial number of water molecules are trapped between the surface of BR and associated OG molecules, presumably with their head groups oriented towards BR.

Finally, we consider the α parameter (see Table 2), which is the contribution to the relaxation rates from sub-nanosecond water motions. The high-frequency excess relaxation rate $\alpha - R_{\text{bulk}}$ is given by a sum of terms of the form $f_i (R_i - R_{\text{bulk}})$, where f_i is the fraction of water molecules with local relaxation rate R_i .²⁹ For a BR-loaded micelle, there are contributions from BR (surface) hydration as well as OG hydration. An estimate of the latter contribution may be obtained from the protein-free sample D2, where $R_1 - R_{\text{bulk}} = 19 \text{ s}^{-1}$. This value is in excellent agreement with the prediction based on the relaxation enhancements of glucose⁴⁹ and of solvent-exposed methylene groups⁵⁰, taking into account that, with a cmc of 35 mM (see above), 30% of the OG molecules are monomeric. Based on the solvent-accessible surface area of the non-buried part of BR, we estimate that about 250 water molecules are in contact with the exposed protein surface. For the surface hydration of previously studied globular proteins, R_i/R_{bulk} ranges from 4.9 to 6.4, with an average of 5.5.^{44,45} Using these values, we obtain $f_{\text{BR}} (R_{\text{BR}} - R_{\text{bulk}}) = 3 \text{ s}^{-1}$. Adding the OG contribution, assumed to be the same as in sample D2, we arrive at $\alpha - R_{\text{bulk}} = 22 \text{ s}^{-1}$, barely half of the experimental value $\alpha - R_{\text{bulk}} = 400 - 352 = 48(\pm 5) \text{ s}^{-1}$. At present, we cannot offer a plausible explanation for this discrepancy.

Discussion

While we have obtained quantitative information about the number of long-lived water molecules and their residence times, the MRD data do not tell us where in the BR molecule these water molecules reside. Nevertheless, the accumulated results of previous MRD studies on numerous proteins^{44,45} clearly show that water molecules with residence times in the range 0.1-10 μs , as found here, must be buried within the protein structure and, thus, may be referred to as internal water molecules. Fortunately, crystal structures of BR are now available at a resolution where most, if not all, of the internal hydration sites occupied by positionally ordered water molecules can be identified.¹⁰⁻¹²

Some caution is warranted in comparing our MRD data, which refer to monomeric BR solubilized by synthetic detergent, with data on BR in the two-dimensional lattice of the purple membrane or the three-dimensional lattice of cubic liquid crystals. In these ordered systems, BR forms trimers with direct protein-protein contacts and each BR molecule is surrounded by about ten ordered native lipid molecules, which appear to interact specifically with the hydrophobic external surface of BR.⁵¹ Nevertheless, despite a lower stability towards thermal denaturation,^{52,53} somewhat altered photocycle kinetics,⁵⁴⁻⁵⁶ and minor structural changes,²⁷ monomeric BR solubilized in detergent micelles is functional²³ and therefore is likely to have essentially the same structure as trimeric BR in the purple membrane.

For reference purposes, we shall use the 1.55 Å structure 1C3W.¹⁰ Among the 23 water molecules reported in this structure, ten have zero solvent-accessible surface area and can thus be considered internal (see Figure 10). The remaining 13 water molecules are highly exposed and therefore cannot have residence times in the range indicated by the MRD data. Of the ten internal water molecules, seven are buried in the EC channel, where they participate in a H-bond network believed to play a central role in the translocation of the excess proton from the retinal Schiff base to the Glu194/Glu204 pair near the extracellular surface of BR.² These seven water molecules, each of which makes two or three strong H-bonds, are also identified in the 1.9 Å structure 1QHJ,¹¹ where an additional water molecule is modeled near the extracellular end of the channel, and in the 2.0 Å structure 1CWQ.¹² Whereas the EC channel is lined with charged and polar residues, the CP channel is largely hydrophobic (with the notable exception of Asp96 in the middle of the CP channel). Only two water molecules have been localized in the CP channel.¹⁰ One of them resides 4.4 Å from the retinal and is present in all three structures. In two of the three structures (1C3W and 1CWQ), a second water molecule is located further towards the cytoplasmic end of the CP channel. Finally, all three structures locate a water molecule in a deep external pocket in the middle of the membrane-spanning part of BR, where it makes three H bonds to the protein. Although not buried within the protein, this water molecule is likely to be long-lived, since it is trapped by lipids (in the purple membrane) or detergents (in the micelle).

Our MRD results require at least seven internal water molecules with residence times in the range 0.1-10 μs (at 4 °C), but would be consistent with a substantially larger number. According to the available crystal structures, BR contains only ten ordered internal water molecules in the ground state. We therefore conclude that at least seven of them, and probably all ten, have residence times in the range 0.1-10 μs . If only seven water molecules have residence times in this range, they must be fully ordered and cannot undergo any flip motions

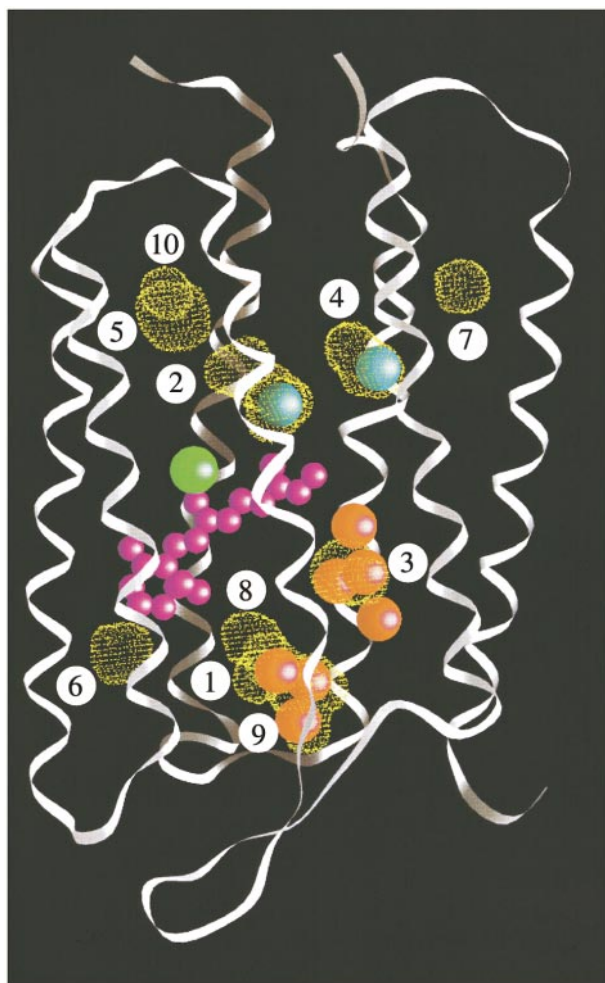


Figure 10. Crystal structure of bacteriorhodopsin (PDB code 1C3W), showing the ten internal water molecules (large spheres) identified at 1.55 Å resolution:¹⁰ seven in the EC channel (red), two in the CP channel (blue), and one water molecule in a surface pocket on the lipid-binding surface (green). The retinal (magenta) is rendered with smaller spheres. The ten cavities described in Table 3 are represented as yellow dot surfaces. The proton is transported from the cytoplasmic side (top) to the extracellular side (bottom).

during their 70 ns correlation time (at 4 °C). Even if all ten internal water molecules contribute to the ^2H dispersion, their (rms) order parameter must be high, $S(^2\text{H}) = 0.88 \pm 0.06$, which leaves little room for fast flip motions.

If, as seems to be the case, the water molecules are highly ordered, with $S(^{17}\text{O}) \approx 1$, then the ^{17}O MRD results indicate that five to seven internal water molecules have residence times in the narrow range 0.1–0.5 μs . It is tempting to identify these with the seven water molecules in the more accessible EC channel, and to identify the one to three additional water molecules required to account for the ^2H dispersion with some or all of the remaining three, more deeply trapped, internal water molecules. This conjecture could be tested by

carrying out MRD experiments on BR mutants lacking one or more of the ten internal water molecules.

On the basis of FTIR-difference spectra for the BR \rightarrow K transition (at 80 K) in samples that had been hydrated by either H_2O , $^2\text{H}_2\text{O}$ or H_2^{18}O , it was concluded that the EC channel contains a water molecule with a residence time of the order of 24 hours.⁵⁷ Water molecules with residence times much longer than 20 μs cannot be detected by ^2H or ^{17}O MRD under the conditions of the present study (see above). Although we cannot exclude the possibility that one or more of the crystallographically identified internal water molecules in BR exchange too slowly to be visible by MRD, we note that internal water residence times longer than milliseconds have not been found in any protein.⁴⁴

To investigate the possibility that the ground-state structure of BR contains additional internal water molecules not detected by X-ray diffraction, we performed a cavity search on the structure 1C3W. This resulted in ten internal cavities large enough to accommodate one or more water molecules (see Figure 10 and Table 3). Although most internal cavities in proteins do not contain crystallographically visible water molecules, Table 3 shows that ground-state BR might contain an additional ten or so hydration sites that escape detection because of low occupancy and/or positional disorder. However, if any such water molecules are not involved in strong directional interactions, they are probably orientationally disordered (small S) as well and might then not contribute significantly to the MRD.

In the M_2 state of the photocycle, there are still seven water molecules in the EC channel (although two of them do not correspond to ground-state hydration sites) but the CP channel, which is more open than in the ground state, now contains six or seven water molecules (as compared to two in the ground state).¹² As compared to the ground state, the M_2 state has larger internal cavities as well as larger invaginations, especially at the cytoplasmic end of the proton channel.¹² Hydration water in these regions might be too disordered to show up in X-ray structures. Furthermore, if the hydration of these cavities and/or invaginations is entropically driven, as expected for non-polar cavities,⁴⁶ then the equilibrium water occupancy might be much lower at 100 K (at which temperature the X-ray structures were determined) than at room temperature. For the same reason, the internal water molecules that were identified by cryocrystallography (in the ground state as well as in excited states of BR) might differ in numbers or positions from the internal water molecules present at room temperature.⁶⁰

The present MRD study was performed on (dark-adapted) ground-state BR and the deduced water exchange kinetics therefore reflect thermal fluctuations from this state. Since the crystallographically identified internal water molecules in

Table 3. Internal cavities in the ground-state BR structure 1C3W

Cavity	Volume ^a (Å ³)	Number of water molecules	
		Potential ^b	Actual ^c
1	88	6	3
2	67	4	1
3	39	2	2 ^d
4	38	2	1
5	31	2	0
6	21	1	0
7	17	1	0
8	17	1	0
9	15	1	0
10	14	1	0

Internal cavities were detected by the program VOIDOO⁵⁸ using 1.2 Å probe radius⁵⁹ and 0.3 Å grid spacing. The atomic coordinates of BR were taken from the structure 1C3W excluding all water molecules. The volume of each detected cavity was computed by reducing the grid spacing to 0.06 Å in 15 cycles. To ensure that all cavities were detected, the procedure was repeated 26 times with the protein translated by 0, 0.1 or 0.2 Å in either of three orthogonal directions.

^a Volume accessible to the surface of the probe sphere.

^b Assuming 14 Å³ per water molecule.

^c For the structure 1C3W.

^d Two additional water molecules are located just outside cavity 3 (see Figure 10).

(light-adapted) ground-state BR are deeply buried, their exchange with bulk water is expected to be rate-limited by conformational fluctuations in the protein. The water residence times reported here therefore imply that substantial conformational fluctuations in the region of the proton channel take place on a time-scale of 0.1-10 μs. It is likely that these fluctuations involve some of the conformational substates that have been identified as intermediates in the photocycle. Most steps in the photocycle are thought to have activation enthalpies of the order of 50 kJ mol⁻¹ in the purple membrane and somewhat less for monomeric detergent-solubilized BR.⁵⁴ This may be compared to the activation enthalpy of 90 kJ mol⁻¹ for the exchange of the most deeply buried water molecule in BPTI, with a mean residence time of 170 μs at 300 K.¹⁶ Assuming an Arrhenius rate law with the same pre-exponential factor as for the BPTI water, the present residence times in the range 0.1-10 μs would correspond to activation enthalpies of 70-80 kJ mol⁻¹. Since this is of the same order of magnitude as typical activation enthalpies for individual steps of the photocycle, the conformational fluctuations that govern the escape of internal water molecules may be as extensive as the conformational changes involved in the photocycle.

The exchange of the Schiff base proton with bulk water protons has been studied by continuous-flow resonance Raman spectroscopy¹⁷ and by ¹H → ¹⁵N solid-state NMR cross-polarization.¹⁸ The Raman study yielded a pH-independent residence time of 2 ms for the Schiff base proton, whereas the NMR study implied a residence time much shorter than 0.5 ms (both values refer to room temperature). These experiments monitor the physical translocation of the proton from the Schiff base to the extracellular bulk solution, a distance of some

20 Å. The rate-limiting step for this process can be either the deprotonation of the Schiff base, presumably by a concerted proton transfer to Asp85 *via* an intervening water molecule (denoted W402 in the crystal structures 1C3W and 1QHJ), or the subsequent movement of the original Schiff base proton, which now resides on W402, out of the EC channel into bulk water. The present MRD results show that most or all water molecules in the EC channel exchange with bulk water on a time-scale shorter than 10 μs, and possibly as fast as 0.1-0.5 μs. Given that the residence time of the Schiff base proton is 2 ms, as indicated by the Raman study,¹⁷ our MRD results suggest that deprotonation of the Schiff base rather than water diffusion through the EC channel is the rate-limiting process. It should be noted that the Raman measurements were carried out on light-adapted BR (with 100% all-*trans* retinal), whereas our MRD measurements were performed on dark-adapted BR (with at least 50% of the 13-*cis*, 15-*syn* retinal isomer). However, this difference is likely to affect the deprotonation rate more than the water dynamics.

In principle, a proton pump like BR could utilize a concerted Grotthuss-type mechanism where the excess proton charge is transported efficiently through a chain of hydrogen-bonded water molecules.⁶¹ According to the high-resolution crystal structure of ground-state BR,¹⁰ however, the seven water molecules in the EC channel do not form contiguous chains longer than two water molecules. Moreover, the positively charged side-chain of Arg82 divides these seven water molecules into two clusters, where every water oxygen atom in one cluster is separated by at least 6 Å from every water oxygen atom in the other cluster. Both the (inferred) topology of the hydrogen bond network and the charge distribution within the EC channel indicate that any concerted proton transfer

should occur from Arg82 to Asp85 or Glu194/204, rather than from Asp85 to Glu194/204 *via* Arg82. Whether proton translocation along the EC channel occurs *via* diffusion of intact hydronium ions or *via* concerted Grotthuss-type proton hopping over a few hydrogen bonds (or a combination of the two), it seems clear that structural fluctuations with concomitant rearrangement of the hydrogen bond network must be rate-limiting. It should also be noted that, even if a hydrogen-bonded water chain did exist in the EC channel, it would affect neither the cited measurements of Schiff base proton exchange nor the water residence times deduced here from ^2H and ^{17}O MRD data. The reason is that these methods probe the actual physical translocation of a given hydrogen (or oxygen) nucleus, whereas, in the Grotthuss mechanism, each hydrogen nucleus moves only a fraction of an Ångström unit when the charge moves over a larger distance. In other words, the hydrogen atom that emerges in the bulk solution is not the same hydrogen atom that just left the Schiff base. (For the same reason, the hydrogen and oxygen nuclei in bulk water have virtually identical self-diffusion coefficients.) In conclusion, the residence times reported here reflect exchange of entire water molecules (or hydronium ions) by processes that are presumably rate-limited by structural fluctuations in the protein.

Materials and Methods

Solubilization of BR

Halobacterium salinarum was grown and purple membrane isolated as described.⁶² The purified bacteriorhodopsin exhibited a 280 nm to 568 nm absorbance ratio of 1.6 for the light-adapted state. Solubilization of BR by *n*-octyl- β -D-glucopyranoside (OG) (Calbiochem) was performed according to Dencher & Heyn,²³ but adapted to the high protein concentration required for the NMR measurements. Purple membranes were suspended at 5 or 13 mg BR ml⁻¹ in 5 mM phosphate buffer (pH 6.9), at a detergent-to-BR ratio of 15 (w/w) and an OG concentration of 664 (sample A) or 255 mM (samples B and C), sonicated for ten seconds in a water-bath sonifier, and thereafter incubated for 72 hours at 4°C in the dark. Upon centrifugation at 200,000 g for 45 minutes to remove non-solubilized material, 64-75% solubilized BR was found in the supernatant. By dialysis against an appropriate volume of detergent-free 5 mM sodium acetate buffer (pH 5.1), for 18 hours, the OG concentration was reduced to 26 mM (sample B), 33 mM (A), or 55 mM (C). Subsequently, BR was concentrated to about 17 (A and C) or 34 mg ml⁻¹ (B) using Centriprep 30 or Centricon YM-30 centrifugal filter devices (Amicon/Millipore) at 1500 g. Samples A and C were dialysed against a 40 mM OG, 5 mM sodium acetate solution (pH 5.1), and thereafter concentrated to (A) 26 or (C) 36 mg BR ml⁻¹. H/ ^2H -exchange by dialysis against 5 mM acetate buffer (pH 5.1), with detergent in the presence of >99.8% $^2\text{H}_2\text{O}$ (Merck) yielded samples with 25 mg BR ml⁻¹ in (A) 40 mM or (C) 37 mM OG, and (B) 32 mg BR ml⁻¹ in 25 mM OG. (BR concentration is based on an extinction coefficient of $4.1 \times 10^4 \text{ M}^{-1} \text{ cm}^{-1}$ at 550 nm, determined from the absorbance changes

during solubilization.) Finally, the solubilized BR samples were adjusted as specified in Table 1.

Preparation of MRD samples

The stock solutions, prepared as described above, were stored in the dark at 4°C. Before starting a series of ^2H MRD experiments, the solution was centrifuged at 14,000 g for 30 minutes to remove aggregated material, whereupon pH* and BR concentration were determined (see Table 1). Samples used for ^{17}O MRD were prepared in the same way, except that ca 300 μl of H_2O enriched to 35 atom% ^{17}O (Cambridge Isotope Laboratories) was added to ca 2 ml of sample. Quoted pH* values are uncorrected for solvent isotope effects. All MRD measurements on BR were carried out with a dark sample at pH* 4.7 and a temperature of either 277.0 or 300.0 K.

The protein concentration was determined spectrophotometrically from the retinal absorbance maximum near 550 nm, using an extinction coefficient of $4.1 \times 10^4 \text{ M}^{-1} \text{ cm}^{-1}$. The OG concentration in the BR-OG solution (sample A2) was determined by integrating the intensity of the three aliphatic peaks (from the 15 protons attached to carbon atoms 2, 3-7, and 8 in the alkyl chain of OG) in the 0.7-1.8 ppm range of the 200 MHz ^1H NMR spectrum. A reference solution of 40 mM OG (determined by weight) in $^2\text{H}_2\text{O}$ at pH* 4.7 (5 mM acetate buffer) was compared with sample A2. The ratio of integrated intensities from the two samples gave an apparent OG concentration of 142 mM in sample A2 and, after correction for the contribution from aliphatic BR protons in this shift range, a real OG concentration of 118(± 6) mM.

MRD measurements

The longitudinal ($R_1 = 1/T_1$) and transverse ($R_2 = 1/T_2$) relaxation rates of the water ^2H and ^{17}O resonances were measured at nine magnetic field strengths in the range 0.38-14.1 T, corresponding to resonance frequencies in the ranges 2.5-92 MHz (^2H) and 2.2-81 MHz (^{17}O). The measurements were performed on several NMR spectrometers with fixed-field cryomagnets (Bruker Avance DMX 100 and 200, Varian Unity 300 and 600) and with a field-variable (0.38-1.83 T) iron-core magnet (Drusch EAR-35N) equipped with field-variable lock and flux stabilizer, and interfaced to a modified Bruker MSL 100 console. Standard inversion recovery (R_1) and spin echo (R_2) pulse sequences were used with an estimated experimental error of 1-2%. The sample temperature was controlled to within ± 0.1 K by a thermostated air flow and was checked before and after each relaxation time measurement with a calibrated thermocouple. The ^2H and ^{17}O relaxation rates of bulk water reference samples with the same water isotope composition as in the protein solutions were measured.

The longitudinal relaxation rate of the water ^2H and OG ^1H magnetizations were measured with the field-cycling (FC) technique in the frequency ranges 3 kHz-1.5 MHz (^2H) and 20 kHz-10 MHz (^1H). For these measurements, we used a Spinmaster Fast Field Cycling Relaxometer (Stelar, Mede, Italy) equipped with a 0.5 T air coil magnet. With the FC technique, R_1 can be measured at very low frequencies (and correspondingly low magnetic fields), where the NMR signal would be undetectably weak in a conventional fixed-field experiment. This is made possible by cyclic variation of the field during the experiment.⁶³ The nuclear spins are first polarized at

a relatively high field; the field is then rapidly switched to a low level where the longitudinal magnetization relaxes towards the new equilibrium value during a variable evolution time. The field is then switched to a high value, where the longitudinal magnetization present at the end of the evolution period is recorded by converting it to observable transverse magnetization with a 90° pulse. When the evolution field is close to the detection field (above 94 mT), the sample is kept in zero field during the polarization period. By repeating this cycle with different evolution times, R_1 can be measured over three decades in frequency. For the ^1H measurements, polarization and detection were done at 10 and 8 MHz, respectively, with switching delays of 10 ms. For the ^2H measurements, polarization and detection were done at 1.2 and 2.8 MHz, respectively, with switching delays of 2 ms and 5 ms. Due to the inferior receptivity of the ^2H isotope, signal averaging was used, with each reported R_1 value being the average of four measurements, each based on 32 field cycles where only the real part of the quadrature-detected signal was recorded. Control measurements on a reference $^2\text{H}_2\text{O}$ sample indicated an experimental accuracy of ca 5%. No deviation from exponential relaxation was detected in either ^2H or ^1H measurements.

MRD data reduction

Non-linear fits of the parameters in the spectral density function in equation (3) were performed with the Levenberg-Marquardt algorithm.⁶⁴ Parameter errors were estimated by the Monte Carlo method,⁶⁴ based on fits to 1000 simulated datasets. The quoted errors correspond to one standard deviation (68% confidence level).

In the case of ^{17}O MRD, joint fits to the combined R_1 and R_2 data were performed without assuming fast-exchange conditions. To an excellent approximation, the spectral density function in equation (3) remains valid, provided that the parameters are reinterpreted. The renormalized parameters are different for R_1 and R_2 . In the case of R_1 , only β_k and τ_{Ck} are renormalized:²⁹

$$\beta'_k = \beta_k(1 + \varepsilon_k)^{-1/2} \quad (7a)$$

$$\tau'_{Ck} = \tau_{Ck}(1 + \varepsilon_k)^{-1/2} \quad (7b)$$

In the case of R_2 , also the α parameter is renormalized:

$$\alpha'' = \alpha + 0.3 \sum_{k=1}^n \beta_k \tau_{Ck} (1 + 0.3\varepsilon_k)^{-1} \quad (8a)$$

$$\beta''_k = \beta_k(1 + 0.3\varepsilon_k)^{-3/2} (1 + \varepsilon_k)^{-1/2} \quad (8b)$$

$$\tau''_{Ck} = \tau_{Ck}(1 + 0.3\varepsilon_k)^{1/2} (1 + \varepsilon_k)^{-1/2} \quad (8c)$$

In equations (7) and (8), we have introduced the dimensionless quantity:

$$\varepsilon_k = R_k^0 \tau_{Wk} = \omega_Q^2 S_k^2 \tau_{Ck} \tau_{Wk} \quad (9)$$

where τ_{Wk} is the water (or labile hydrogen) residence time.

Since ^{17}O has nuclear spin quantum number $I = 5/2$, it really has tri-exponential longitudinal and transverse relaxation.²⁹ However, due to the large frequency-independent part (α) of the spectral density, the relaxation

becomes effectively exponential with R_1 and R_2 given by the same equations (1) and (2) as for ^2H (with spin $I = 1$).⁶⁵ For the parameter values of interest here, the error introduced by this approximation is within the measurement error.

Acknowledgments

In Lund, we thank Vladimir Denisov, Esteban Anorado (Stelar s.n.c.), and Kandadai Venu (University of Hyderabad) for advice and help with NMR instruments. In Darmstadt, we are indebted to Christine Schröpfer and Holger Seelert for their help with sample preparation. This work was supported by the Crafoord Foundation and the Swedish Natural Science Research Council (to B.H.) and by the Deutsche Forschungsgemeinschaft, SFB 472 (to N.A.D.).

References

- Haupts, U., Tittor, J. & Oesterhelt, D. (1999). Closing in on bacteriorhodopsin: progress in understanding the molecule. *Annu. Rev. Biophys. Biomol. Struct.* **28**, 367-399.
- Lanyi, J. K. (1999). Progress toward an explicit mechanistic model for the light-driven pump, bacteriorhodopsin. *FEBS Letters*, **464**, 103-107.
- Heberle, J., Fitter, J., Sass, H. J. & Büldt, G. (2000). Bacteriorhodopsin: the functional details of a molecular machine are being resolved. *Biophys. Chem.* **85**, 229-248.
- Lanyi, J. K. (2000). Molecular mechanism of ion transport in bacteriorhodopsin: insights from crystallographic, spectroscopic, kinetic, and mutational studies. *J. Phys. Chem. sect. B*, **104**, 11441-11448.
- Dencher, N. A., Sass, H. J. & Büldt, G. (2000). Water and bacteriorhodopsin: structure, dynamics, and function. *Biochim. Biophys. Acta*, **1460**, 192-203.
- Kandori, H. (2000). Role of internal water molecules in bacteriorhodopsin. *Biochim. Biophys. Acta*, **1460**, 177-191.
- Luecke, H. (2000). Atomic resolution structures of bacteriorhodopsin photocycle intermediates: the role of discrete water molecules in the function of this light-driven ion pump. *Biochim. Biophys. Acta*, **1460**, 133-156.
- Papadopoulos, G., Dencher, N. A., Zaccari, G. & Büldt, G. (1990). Water molecules and exchangeable hydrogen ions at the active centre of bacteriorhodopsin localized by neutron diffraction. *J. Mol. Biol.* **214**, 15-19.
- Hauss, T., Papadopoulos, G., Verclas, S. A. W., Büldt, G. & Dencher, N. A. (1997). Neutron diffraction on purple membranes. Essential water molecules in the light-driven proton pump bacteriorhodopsin. *Physica sect. B*, **234-236**, 217-219.
- Luecke, H., Schobert, B., Richter, H.-T., Cartailier, J.-P. & Lanyi, J. K. (1999). Structure of bacteriorhodopsin at 1.55 Å resolution. *J. Mol. Biol.* **291**, 899-911.
- Belrhali, H., Nollert, P., Royant, A., Menzel, C., Rosenbusch, J. P., Landau, E. M. & Pebay-Peyroula, E. (1999). Protein, lipid and water organization in bacteriorhodopsin crystals: a molecular view of the purple membrane at 1.9 Å resolution. *Structure*, **7**, 909-917.

12. Sass, H. J., Büldt, G., Gessenich, R., Hehn, D., Neff, D. & Schlesinger, R. *et al.* (2000). Structural alterations for proton translocation in the M state of wild-type bacteriorhodopsin. *Nature*, **406**, 649-652.
13. Luecke, H., Schobert, B., Richter, H.-T., Cartailler, J.-P. & Lanyi, J. K. (1999). Structural changes in bacteriorhodopsin during ion transport at 2 Å resolution. *Science*, **286**, 255-260.
14. Edman, K., Nollert, P., Royant, A., Belrhali, H., Pebay-Peyroula, E. & Hajdu, J. *et al.* (1999). High-resolution X-ray structure of an early intermediate in the bacteriorhodopsin photocycle. *Nature*, **401**, 822-826.
15. Royant, A., Edman, K., Ursby, T., Pebay-Peyroula, E., Landau, E. M. & Neutze, R. (2000). Helix deformation is coupled to vectorial proton transport in the photocycle of bacteriorhodopsin. *Nature*, **406**, 645-648.
16. Denisov, V. P., Peters, J., Hörlein, H.-D. & Halle, B. (1996). Using buried water molecules to explore the energy landscape of proteins. *Nature Struct. Biol.* **3**, 505-509.
17. Deng, H., Huang, L., Callender, R. & Ebrey, T. (1994). Evidence for a bound water molecule next to the retinal Schiff base in bacteriorhodopsin and rhodopsin: a resonance Raman study of the Schiff base hydrogen/deuterium exchange. *Biophys. J.* **66**, 1129-1136.
18. Harbison, G. S., Roberts, J. E., Herzfeld, J. & Griffin, R. G. (1988). Solid-state NMR detection of proton exchange between the bacteriorhodopsin Schiff base and bulk water. *J. Am. Chem. Soc.* **110**, 7221-7223.
19. Engelhard, M. & Bechinger, B. (1995). Application of NMR spectroscopy to retinal proteins. *Israel J. Chem.* **35**, 273-288.
20. Saito, H., Tuzi, S., Yamaguchi, S., Tanio, M. & Naito, A. (2000). Conformation and backbone dynamics of bacteriorhodopsin revealed by ¹³C NMR. *Biochim. Biophys. Acta*, **1460**, 39-48.
21. Herzfeld, J. & Toung, B. (2000). NMR probes of vectoriality in the proton-motive photocycle of bacteriorhodopsin: evidence for an "electrostatic steering" mechanism. *Biochim. Biophys. Acta*, **1460**, 95-105.
22. Lechner, R. E., Dencher, N. A., Fitter, J. & Dippel, Th. (1994). Two-dimensional proton diffusion on purple membrane. *Solid State Ionics*, **70/71**, 296-304.
23. Dencher, N. A. & Heyn, M. P. (1982). Preparation and properties of monomeric bacteriorhodopsin. *Meth. Enzymol.* **88**, 5-10.
24. Seigneuret, M., Neumann, J.-M. & Rigaud, J.-L. (1991). Detergent delipidation and solubilization strategies for high-resolution NMR of the membrane protein bacteriorhodopsin. *J. Biol. Chem.* **266**, 10066-10069.
25. Seigneuret, M., Neumann, J.-M., Levy, D. & Rigaud, J.-L. (1991). High-resolution ¹³C NMR study of the topography and dynamics of methionine residues in detergent-solubilized bacteriorhodopsin. *Biochemistry*, **30**, 3885-3892.
26. Patzelt, H., Ulrich, A. S., Egbringhoff, H., Düx, P., Ashurst, J. & Simon, B. *et al.* (1997). Towards structural investigations on isotope labelled native bacteriorhodopsin in detergent micelles by solution-state NMR spectroscopy. *J. Biomol. NMR*, **10**, 95-106.
27. Tanio, M., Tuzi, S., Yamaguchi, S., Konishi, H., Naito, A., Needleman, R. *et al.* (1998). Evidence of local conformational fluctuations and changes in bacteriorhodopsin, dependent on lipids, detergents, and trimeric structure, as studied by ¹³C NMR. *Biochim. Biophys. Acta*, **1375**, 84-92.
28. Otting, G. (1997). NMR studies of water bound to biological molecules. *Prog. NMR Spectrosc.* **31**, 259-285.
29. Halle, B., Denisov, V. P. & Venu, K. (1999). Multi-nuclear relaxation dispersion studies of protein hydration. In *Biological Magnetic Resonance* (Krishna, N. R. & Berliner, L. J., eds), vol. 17, pp. 419-484, Kluwer/Plenum, New York.
30. Halle, B. & Denisov, V. P. (2001). Magnetic relaxation dispersion studies of biomolecular solutions. *Methods Enzymol.* **338**, 178-201.
31. Schauer, G., Kimmich, R. & Nusser, W. (1988). Deuteron field-cycling relaxation spectroscopy and translational water diffusion in protein hydration shells. *Biophys. J.* **53**, 397-404.
32. Kameyama, K. & Takagi, T. (1990). Micellar properties of octylglucoside in aqueous solution. *J. Coll. Interf. Sci.* **137**, 1-10.
33. Tanford, C. (1980). *The Hydrophobic Effect*, 2nd edit., Wiley, New York.
34. Nilsson, F., Söderman, O. & Johansson, I. (1996). Physical-chemical properties of the *n*-octyl-β-D-glucoside/water system. A phase diagram, self-diffusion NMR, and SAXS study. *Langmuir*, **12**, 902-908.
35. Frindi, M., Michels, B. & Zana, R. (1992). Ultrasonic absorption studies of surfactant exchange between micelles and bulk phase in aqueous micellar solutions of nonionic surfactants with a short alkyl chain. 3. Surfactants with a sugar head group. *J. Phys. Chem.* **96**, 8137-8141.
36. Belmajdoub, A., Diter, B. & Canet, D. (1986). Multi-field proton longitudinal relaxation measurements for the determination of correlation times in surfactant aggregates. *Chem. Phys. Letters*, **131**, 426-429.
37. Halle, B. (1996). Spin dynamics of exchanging quadrupolar nuclei in locally anisotropic systems. *Prog. NMR Spectrosc.* **28**, 137-159.
38. Miercke, L. J. W., Betlach, M. C., Mitra, A. K., Shand, R. F., Fong, S. K., Stroud, R. M. & Kliger, D. S. (1991). Wild-type and mutant bacteriorhodopsin D85N, D96N, and R82Q: purification to homogeneity, pH dependence of pumping, and electron diffraction. *Biochemistry*, **30**, 3088-3098.
39. Hills, B. P. (1991). Multinuclear NMR studies of water in solutions of simple carbohydrates. I. Proton and deuterium relaxation. *Mol. Phys.* **72**, 1099-1121.
40. Halle, B. (1991). Theory of spin relaxation by diffusion on curved surfaces. *J. Chem. Phys.* **94**, 3150-3168.
41. Clymer, J. W. & Ragle, J. L. (1982). Deuterium quadrupole coupling in methanol, salicylic acid, catechol, resorcinol, and hydroquinone. *J. Chem. Phys.* **77**, 4366-4373.
42. Wendt, M. A., Zeidler, M. D. & Farrar, T. C. (1999). The temperature dependence of the deuterium quadrupole coupling constant and the molecular rotational correlation time in liquid methanol. *Mol. Phys.* **97**, 753-756.
43. Denisov, V. P. & Halle, B. (1995). Hydrogen exchange and protein hydration: the deuteron spin relaxation dispersions of bovine pancreatic trypsin inhibitor and ubiquitin. *J. Mol. Biol.* **245**, 698-709.
44. Halle, B. (1998). Water in biological systems: the NMR picture. In *Hydration Processes in Biology* (Bellissent-Funel, M.-C., ed.), pp. 233-249, IOS Press, Dordrecht.

45. Denisov, V. P. & Halle, B. (1996). Protein hydration dynamics in aqueous solution. *Faraday Discuss.* **103**, 227-244.
46. Denisov, V. P., Venu, K., Peters, J., Hörlein, H.-D. & Halle, B. (1997). Orientational disorder and entropy of water in protein cavities. *J. Phys. Chem. sect. B*, **101**, 9380-9389.
47. Chang, C.-H., Chen, J.-G., Govindjee, R. & Ebrey, T. (1985). Cation binding by bacteriorhodopsin. *Proc. Natl Acad. Sci. USA*, **82**, 396-400.
48. Váró, G., Brown, L. S., Needleman, R. & Lanyi, J. K. (1999). Binding of calcium ions to bacteriorhodopsin. *Biophys. J.* **76**, 3219-3226.
49. Uedaira, H., Ikura, M. & Uedaira, H. (1989). Natural abundance oxygen-17 magnetic relaxation in aqueous solutions of carbohydrates. *Bull. Chem. Soc. Japan*, **62**, 1-4.
50. Ishihara, Y., Okouchi, S. & Uedaira, H. (1997). Dynamics of hydration of alcohols and diols in aqueous solution. *J. Chem. Soc. Faraday Trans.* **93**, 3337-3342.
51. Krebs, M. P. & Isenbarger, T. A. (2000). Structural determinants of purple membrane assembly. *Biochim. Biophys. Acta*, **1460**, 15-26.
52. Broulliette, C. G., McMichens, R. B., Stern, L. J. & Khorana, H. G. (1989). Structure and thermal stability of monomeric bacteriorhodopsin in mixed phospholipid/detergent micelles. *Proteins: Struct. Funct. Genet.* **5**, 38-46.
53. Mukai, Y., Kamo, N. & Mitaku, S. (1999). Light-induced denaturation of bacteriorhodopsin solubilized by octyl- β -glucoside. *Protein Eng.* **12**, 755-759.
54. Váró, G. & Lanyi, J. K. (1991). Effects of the crystalline structure of purple membrane on the kinetics and energetics of the bacteriorhodopsin photocycle. *Biochemistry*, **30**, 7165-7171.
55. Milder, S. J., Thorgeirsson, T. E., Miercke, L. J. W., Stroud, R. M. & Kliger, D. S. (1991). Effects of detergent environments on the photocycle of purified monomeric bacteriorhodopsin. *Biochemistry*, **30**, 1751-1761.
56. Lopez, F., Lobasso, S., Colella, M., Agostiano, A. & Corcelli, A. (1999). Light-dependent and biochemical properties of two different bands of bacteriorhodopsin isolated on phenyl-Sepharose CL-4B. *Photochem. Photobiol.* **69**, 599-604.
57. Fischer, W. B., Sonar, S., Marti, T., Khorana, H. G. & Rothschild, K. J. (1994). Detection of a water molecule in the active site of bacteriorhodopsin: hydrogen bonding changes during the primary photoreaction. *Biochemistry*, **33**, 12757-12762.
58. Kleywegt, G. J. & Jones, T. A. (1994). Detection, delineation, measurement and display of cavities in macromolecular structures. *Acta Crystallog. sect. D*, **50**, 178-185.
59. Hubbard, S. J. & Argos, P. (1995). Detection of internal cavities in globular proteins. *Protein Eng.* **8**, 1011-1015.
60. Scheidig, A. J., Burmester, C. & Goody, R. S. (1999). The pre-hydrolysis state of p21^{ras} in complex with GTP: new insights into the role of water molecules in the GTP hydrolysis reaction of ras-like proteins. *Structure*, **7**, 1311-1324.
61. Gutman, M. & Nachliel, E. (1997). Time-resolved dynamics of proton transfer in proteinous systems. *Annu. Rev. Phys. Chem.* **48**, 329-356.
62. Bauer, P.-J., Dencher, N. A. & Heyn, M. P. (1976). Evidence for chromophore-chromophore-interactions in the purple membrane from reconstitution experiments of the chromophore-free membrane. *Biophys. Struct. Mechanism*, **2**, 79-92.
63. Noack, F. (1986). NMR field-cycling spectroscopy: principles and applications. *Prog. NMR Spectrosc.* **18**, 171-276.
64. Press, W. H., Teukolsky, S. A., Vetterling, W. T. & Flannery, B. P. (1992). *Numerical Recipes in C. The Art of Scientific Computing*, 2nd edit., Cambridge University Press, Cambridge, UK.
65. Halle, B. & Wennerström, H. (1981). Nearly exponential quadrupolar relaxation. A perturbation treatment. *J. Magn. Reson.* **44**, 89-100.

Edited by P. E. Wright

(Received 22 January 2001; received in revised form 18 June 2001; accepted 18 June 2001)